OPTICA

# Coherent control in quartz-enhanced photoacoustics: fingerprinting a trace gas at ppm-level within seconds

Simon Angstenberger,* Moritz Floess, Luca Schmid, Pavel Ruchka, Tobias Steinle, and Harald Giessen

*4th Physics Institute and Stuttgart Research Center of Photonic Engineering, University of Stuttgart, Pfaffenwaldring 57, 70569 Stuttgart, Germany*
**simon.angstenberger@pi4.uni-stuttgart.de*

*Received 9 October 2024; revised 14 November 2024; accepted 17 November 2024; published 9 January 2025*

**Quartz-enhanced photoacoustic spectroscopy (QEPAS) has become a versatile tool for detection of trace gases at extremely low concentrations, leveraging the high quality (Q)-factor of quartz tuning forks. However, this high Q-factor imposes an intrinsic spectral resolution limit for fast wavelength sweeping with tunable laser sources due to the long ringing time of the tuning fork. Here, we introduce a technique to coherently control and damp the tuning fork by phase-shifting the modulation sequences of the driving laser. Particularly, we send additional laser pulses into the photoacoustic cell with a timing that corresponds to a $\pi$ phase shift with respect to the tuning fork oscillation, effectively stopping its oscillatory motion. This enables acquisition of a complete methane spectrum spanning 3050–3450 nm in just three seconds, preserving the spectral shape. Our measured data is in good agreement with the theoretically expected spectra from the HITRAN database when convolved with the laser linewidth of $<2\,\mathrm{cm}^{-1}$. This will leverage the use of QEPAS with fast-sweeping OPOs in real-world gas sensing applications beyond laboratory environments with extremely fast acquisition speed enabled by our coherent control scheme.**



https://doi.org/10.1364/OPTICA.544448

Monitoring of trace gases is an important task in environmental sensing, medical physics, and industrial applications [1,2]. The potential of photoacoustic spectroscopy to sense low concentrations has only been fully realized in recent decades, despite its origins dating back over a century [3].

This trend can largely be attributed to the employment of quartz tuning forks (QTFs) instead of microphones for acoustic detection. Their use has enabled quartz-enhanced photoacoustic spectroscopy (QEPAS) as a robust spectroscopic technique [4] with the possibility to detect trace gases at very low concentrations down to the parts-per-trillion range [5,6]. The pressure wave generated by the photoacoustic effect moves the prongs of the fork. The high Q-factor of QTFs in QEPAS then enables greatly enhanced sensitivities compared to conventional photoacoustic spectroscopy.

Its sensitivity, compactness [7], and the capability to operate without bulky gas cells or complex optical alignment render QEPAS a promising candidate for sensing low gas concentrations. This is important for detection of gases that are toxic or a have huge environmental impact even at low concentrations.

However, most systems are limited to a distinct gas species as the most common laser sources for generating the photoacoustic effect are laser diodes and quantum cascade lasers. They are ideal to address a distinct spectral absorption feature of a molecule as their spectral output is narrowband (few to below single-digit $\mathrm{cm}^{-1}$) [8]. Yet the tunability of both systems is highly limited, allowing only a small range of accessible wavelengths and measurement of one particular trace gas [9,10]. This makes setups for multiple gas species rather bulky, employing stacked diodes and multiple QEPAS cells that demand considerable alignment and gas distribution effort [11–14]. Even then, it does not allow for rapid tunability. Neither is it possible to distinguish two gas species that are resonant at the same wavelength.

Employing optical parametric oscillators (OPOs) enables wavelength tuning across a broad range [15,16] and has already been used in QEPAS [17–19]. However, the quality factor of the QTF limits the applicability of QEPAS in combination with swept sources: as one sweeps the wavelength across a strong resonance, there will be residual oscillations even far off the actual resonance. At fast tuning speeds, this smears out the spectral features and makes it almost impossible to deduce the actual spectral shape, shown by Christensen *et al.* in 2020 [20]. If the gas constituents are unknown or their relative absorption strength differs significantly, it is nevertheless necessary to scan a large wavelength range to uniquely determine the gas species from its spectral shape ('fingerprint'). Sweep times of 30 minutes are necessary to acquire the full spectral information of methane.

In this Letter, we introduce a novel method, namely, coherent control QEPAS (COCO-QEPAS), that damps the fork and thus significantly decreases spectral acquisition times in QEPAS without compromising sensitivity while conserving the spectral shape. We excite the fork by a sequence of intensity-modulated laser light and dampen it by a phase-shifted successive sequence.

In this manner, we acquire a full methane spectrum from 3150 to 3450 nm within three seconds, keeping excellent agreement to theoretical data from the HITRAN database [21,22]. Our approach reduces the overall acquisition time by more than an order of magnitude for spectral data without being restricted to a certain gas species. Our method will transfer QEPAS from the lab to the application stage by overcoming intrinsic spectral resolution limits in real-time monitoring.

The measurement principle and setup are laid out in Fig. 1. A FFOPO generates a narrowband output from 1400 to 4000 nm. Although the picosecond output of the FFOPO (Stuttgart Instruments PIANO) is pulsed at 50 MHz, it can be treated as a quasi continuous wave for the means of our experiment as the timescale of the acoustic response is about four orders of magnitude larger. To match the acoustic resonance, the FFOPO output is intensity modulated using an acousto-optic modulator (AOM). The beam is then sent into a QEPAS gas cell (Thorlabs, ADM01).

The AOM modulation frequency (12420 Hz) is matched to the fundamental resonance of the QTF in the gas cell. When the tunable laser wavelength matches an absorption feature of the trace gas, sound waves are generated by the photoacoustic effect. They resonantly enhance the oscillatory motion of the fork in each cycle. The piezoelectric fork translates the mechanical oscillation to a voltage signal. Lock-in detection filters noise contributions far from the oscillation frequency (UHFLI, Zurich Instruments).

This process is already sensitive to trace gases at the ppm-level. However, while the high Q-factor of the fork's resonance enables high sensitivities in the ppm-range in the first place, it is also the limiting factor for rapid acquisition of spectra: after driving the fork by the laser-gas interaction, it will continue to oscillate, illustrated by the upper graph in Fig. 1(b). Residual signal then disturbs the measurement at the next wavelength position and leads to aliasing. Note that $\tau = 190$ ms only indicates the 1/e decay. Even after that time, there is still signal left.

By employing a coherent control scheme, we can overcome this intrinsic limitation. The principle is laid out in the lower panels of Fig. 1(b). First, initial excitation of the fork happens by photoacoustic events (Excitation). These events are initiated by resonant laser pulses and marked as explosions on the amplitude graph. This sequence is in phase with the fork's movement, like pushing a kid on a swing. After excitation, the oscillation strength is measured (Measurement). Subsequently, a second sequence of pulses dampens the fork coherently (Coherent control). While the excitation sequence is in phase with the fork's movement, the damping sequence is phase-shifted. The prongs of the fork move inwards while the pressure wave moves outwards. This stops the forks motion, just as one stops a kid on a swing by a ($\pi$-) phase-shifted application of the driving force. The pressure wave and resulting force still act via the same process. The only difference is the phase relative to the motion.

The phase difference is controlled by an arbitrary waveform generator, which is synchronized to the same oscillator as the lock-in detection. In this manner, we achieve uniform electronic control. From the analogy, one would guess that for ideal damping the phase should be shifted by $\pi$, as the damping force and oscillatory motion are antisymmetric. We verify this by varying the phase shift between excitation and damping cycle in Fig. 2. Exemplary snippets of the incoming modulated laser pulses are depicted in Fig. 2(a), where the signal output of the FFOPO is recorded with a photodiode, while the idler drives the acoustic interaction in the

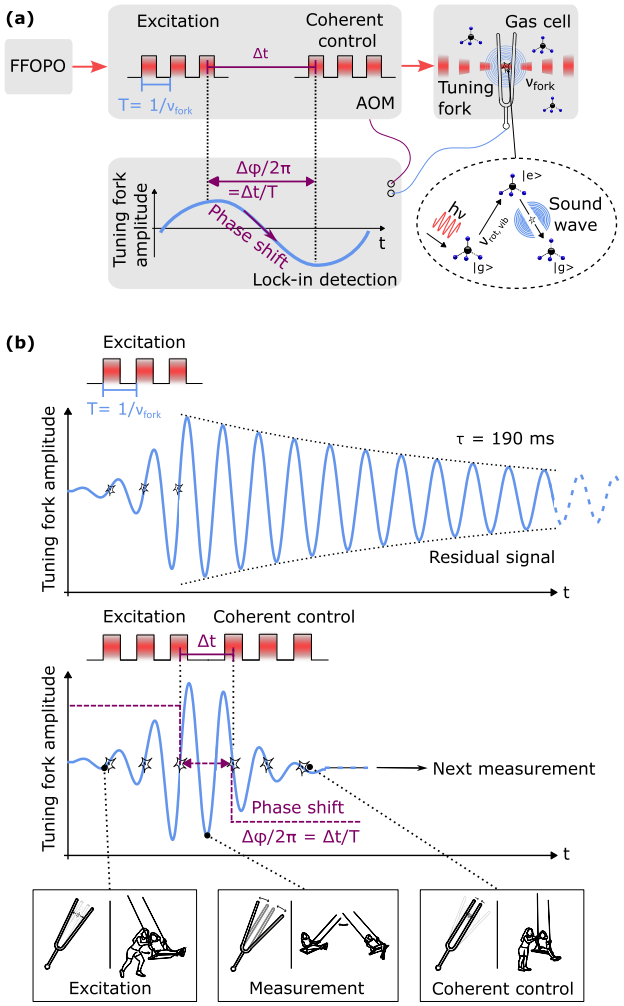


**Fig. 1.** Measurement principle of coherently controlled quartz-enhanced photoacoustic spectroscopy (COCO-QEPAS). (a) Setup scheme for COCO-QEPAS. The tunable laser light of a fiber-feedback optical parametric oscillator (FFOPO) is modulated by means of an acousto-optic modulator (AOM). At absorptive wavenumbers $\nu_{\mathrm{vib,rot}}$, this excites the fork at its modulation frequency. A coherent control pulse sequence is phase-shifted by $\Delta\phi$. (b) Residual oscillation of the fork due to its high Q-factor after excitation. Coherent control allows deceleration of the fork. First, the fork is accelerated (Excitation). Then, the oscillation amplitude reveals spectral information (Measurement). Eventually, the fork is actively damped (Coherent control), enabling a fast next measurement.

cell. The pulse peaks are cropped to enhance the reader's focus on the crucial timing difference rather than pulse heights. The idler output in this measurement is tuned to the main resonance of $CH_4$ at 3314 nm. 50 cycles are used for both excitation and damping of the fork. As mentioned above, the modulation frequency of these pulses lies at 12420 Hz, corresponding to an oscillatory period of 80.5 µs. We vary the phase shift between excitation sequence and damping sequence from 0 to $2\pi$, which is color-coded in blue (no shift), gray ($\pi$ shift), to red ($2\pi$ shift) for all subfigures.

Figures 2(b) and 2(c) show the resulting cell signal when demodulated with the lock-in with an integration time of 80 µs, corresponding to one oscillation period of the fork. The curves are plotted for integer multiples of $\pi/6$ and depicted with thicker linewidths for sequences matching the cases of Fig. 2(a). In the case of no phase shift (blue curve), the damping sequence is *de facto*

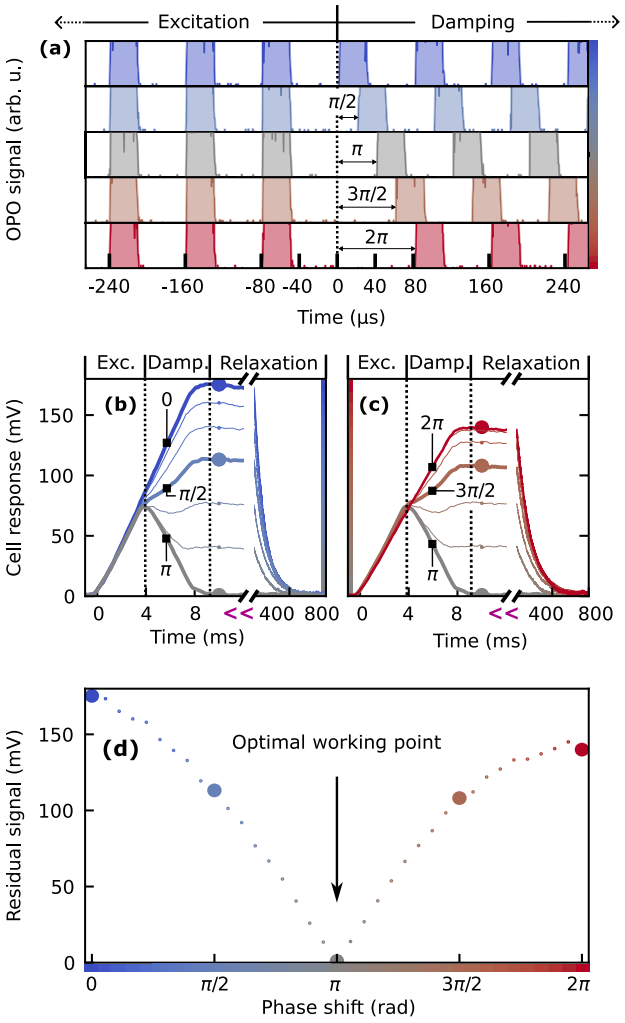


**Fig. 2.** Residual signal dependent on the phase shift between excitation and damping sequence. (a) Modulated laser power. The phase shift between excitation and damping cycles is color-coded in blue (0) to red ($2\pi$). (b) Time trace of the demodulated cell signal for exciting with a sequence of 50 cycles and phase shifts of 50 damping cycles from 0 to $\pi$. The remaining residual cell signal at 10 ms is minimal for a phase shift of $\pi$. (c) Demodulated cell signal for further increasing the phase shift to $2\pi$. In (d) the dependence of the residual signal on the phase shift is plotted. No residual signal is left at $\pi$.

an extension of the excitation sequence to 100 pulses. The signal increases linearly to 175 mV. Then the fork continues to oscillate and only very slowly decreases. The residual amplitude, indicated by a dot, is recorded after 10 ms. The complete relaxation process extends beyond 400 ms. Increasing the phase shift yields a smaller increase of the amplitude during the damping sequence. In case of the light blue curve ($\pi/2$ shift), the phase of the fork oscillation gradually realigns with the phase of the damping cycle before increasing again. This case corresponds to the sequences in the second row of Fig. 2(a). The residual signal level decreases for phase shifts closer to $\pi$. Exactly at $\pi$ [cf. middle row of Fig. 2(a), gray], the damping sequence decreases the signal in the same manner that the excitation increases it. In this way it is possible to reduce the residual signal to 0 mV after 10 ms. The behavior for further increase of the phase shift from $\pi$ onwards is depicted in Fig. 2(c) [corresponding sequence: two lower rows of Fig. 2(a)]. The curves for phase shifts above $\pi$ are analogous to phase shifts below $\pi$. For non-integer multiples of $\pi$, a kink indicates re-establishing of a $\pi/2$ phase between driving force and oscillation. We assume that the lower overall values for $2\pi$ stem from a slight change in gas pressure or a drift of the resonance frequency over the course of the measurement (approx. 3 h). The residual signal is plotted over the phase shift between excitation and damping sequence in Fig. 2(d). Data for the residual signal of the intermediate steps, shown as smaller dots, can be found in Fig. S1 in Supplement 1. The optimal working point is found exactly at $\pi$, and the increasing residual signal is symmetric around the optimum.

With the validity of our concept at hand, we now implement this damping routine for fast spectral acquisition of trace gas data. The principle has already been laid out in the bottom panels of Fig. 1. The laser is set to a certain wavelength. The first sequence excites the fork. Then, the laser is turned off for two cycles and the amplitude of the oscillation is measured by triggering a read-out of the lock-in amplifier. Therefore, post-processing of the data is not necessary. After measuring, the fork is decelerated by the phase-shifted coherent control sequence. Immediately after that the FFOPO output is swept to the next wavelength position, where the fork is again excited by a sequence that is in phase with the previous excitation sequence; see Fig. S2 for details on the sequence.

Figure 3 depicts data acquisition with conventional sweeping and permanent modulation of the signal, i.e., permanent excitation in the left panels of Fig. 3(a). The results of COCO-QEPAS are plotted in the right panels of Fig. 3(a). In conventional QEPAS, the residual oscillations of the fork become increasingly visible especially on the Q-branch (main peak) of the spectra. At fast tuning speeds, the (temporal) exponential decay after excitation of the Q-branch is visible. Even more drastic for actual identification of a given trace gas is the smearing out of the spectral features on the P- and R-branches. At the same sweeping speeds, the spectral features do no change visibly for COCO-QEPAS. Even at an acquisition time of only three seconds, the whole branch is still resolved well.

Although the enhancement is clearly visible by eye, we now quantify the deviation of the spectral shape. As a reference, we use the theoretically expected data by convolving the data from the HITRAN database with the laser linewidth. The linewidth was measured in steps of 50 nm and is interpolated in between for the convolution (see Fig. S3 for the recorded spectra). As the signal-to-noise ratio (SNR) and the normalized noise equivalent absorption coefficient (NNEA) [20] only compare the height of a peak (here, on the Q-branch) to a noise base level, they under-estimate the smearing of spectral features. Therefore, we define a figure of merit $D$, which quantifies the deviation of the measured spectral shape from the theoretical one. Specifically, $D$ is calculated by summing the quadratic deviations for every measurement $i$ of the normalized measured intensity $I_{\mathrm{i,PAS}}$ from the normalized expected intensity $I_{\mathrm{i,HITRAN}}$ for all $n$ measurements as

$$D = \frac{1}{n}\sum_{i}^{n}\left(I_{\mathrm{i,PAS}} - I_{\mathrm{i,HITRAN}}\right)^2. \quad (1)$$

The deviation for both methods is displayed in Fig. 3(b). The quantitative analysis shows that conventional QEPAS suffers from an increasing deviation for higher tuning speeds. In contrast, the increase in deviation for coherent control is an order of magnitude less. All spectral data is calibrated to the slowest sweep speed by mapping the experimental wavelength to the theoretical one using a linear interpolation; see Fig. S4.

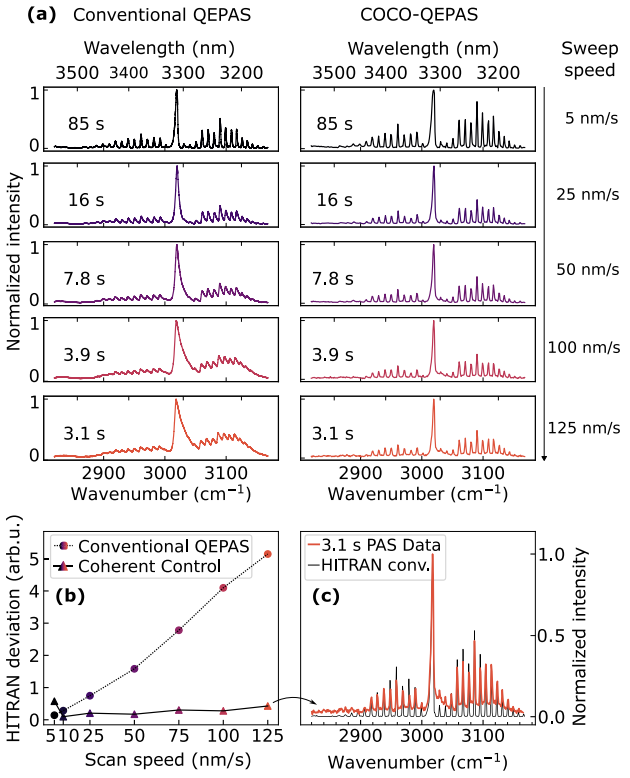


**Fig. 3.** Comparison of COCO-QEPAS with conventional QEPAS. (a) Acquisition of $CH_4$ spectra at increasing sweeping speeds from 5 to 125 nm/s. The fork relaxation time reflects in increasingly smeared out spectral features at higher sweeping speeds. COCO-QEPAS overcomes this detrimental effect. (b) Quantification of improved spectral quality in coherent control by the quadratic deviation from the convolved HITRAN data. (c) Fastest COCO-QEPAS sweep in three seconds (orange) overlapped with HITRAN data. The spectral features are still visible for all branches.

Figure 3(c) displays a comparison of the fastest acquired spectrum to convolved HITRAN data. Relative strengths of the peaks are matched well, and the linewidth is conserved. To reference this to other trace gas measurements, we state an SNR of 146 and thus an NNEA of $3.7 \times 10^{-9}$ W cm$^{-1}$ Hz$^{-1/2}$ for the fastest COCO-QEPAS sweep. Additional spectra and comparison to HITRAN at all speeds are shown in Fig. S5. The sampling of one sequence is half of the laser linewidth in accordance to the Shannon-Nyquist theorem [23]. This is an optimal compromise between lower signal for narrower sampling (not enough cycles to excite the fork) and smeared out spectral features for broad sampling. Details are presented in Fig. S2.

In practice, the fastest tuning speeds only allow continuous tuning and thus the wavelength slightly changes over the course of one excitation cycle. Contrary to intuition, this does not affect the accuracy of our measurement greatly. We demonstrate this by comparing sweeping in both directions, shown in Fig. S6. Note that a sweep speed of up to 125 nm/s in this spectral region is, to the best of the authors' knowledge, unprecedented.

In this letter, a novel method for fast and precise acquisition of spectral data is presented. Coherent damping of the residual oscillation of the quartz tuning fork inside a QEPAS cell prevents spectral features from smearing out and keeps the spectral shape in good agreement to the theoretical HITRAN data. Coherent control renders fast-sweeping narrowband OPOs, a powerful tool for photoacoustic spectroscopy in a wide range of applications: one setup is sufficient to characterize several trace gases simultaneously, enabling QEPAS as a measurement technique beyond optical laboratories [20]. Potential applications include petrochemical sensing, breath analysis, and quantification of greenhouse gas emissions [5,7,13].

**Funding.** Bundesministerium für Bildung und Forschung (KMU MIRSWEEP); European Research Council (PoC 3DPRINTEDOPTICS); Carl-Zeiss-Stiftung; Deutsche Forschungsgemeinschaft (431314977/GRK2642); Center for Integrated Quantum Science and Technology; Baden-Württemberg Stiftung.

**Acknowledgment.** S. Angstenberger would like to thank Mario Hentschel for many fruitful discussions and Theelke Kobuch for providing the illustrations of tuning forks and oscillatory motions.

**Disclosures.** The authors declare no conflicts of interest.

**Data availability.** Data underlying the results presented in this paper are not publicly available at this time but may be obtained from the authors upon reasonable request.

**Supplemental document.** See Supplement 1 for supporting content.

## REFERENCES

1. P. Luo, J. Harrist, G. Menduni, *et al.*, ACS Omega **7**, 3395 (2022).
2. T. Strahl, J. Herbst, A. Lambrecht, *et al.*, Appl. Opt. **60**, C68 (2021).
3. C. Haisch, Meas. Sci. Technol. **23**, 12001 (2011).
4. A. A. Kosterev, Y. A. Bakhirkin, R. F. Curl, *et al.*, Opt. Lett. **27**, 1902 (2002).
5. V. Spagnolo, P. Patimisco, S. Borri, *et al.*, Opt. Lett. **37**, 4461 (2012).
6. T. Tomberg, M. Vainio, T. Hieta, *et al.*, Sci. Rep. **8**, 1 (2018).
7. F. Sgobba, A. Sampaolo, P. Patimisco, *et al.*, Photoacoustics **25**, 100318 (2022).
8. M. Germer and M. Wolff, Appl. Opt. **48**, B80 (2009).
9. R. Lewicki, G. Wysocki, A. A. Kosterev, *et al.*, Opt. Express **15**, 7357 (2007).
10. Y. Ma, G. Yu, J. Zhang, *et al.*, J. Opt. **17**, 55401 (2015).
11. L. Dong, A. A. Kosterev, D. Thomazy, *et al.*, Proc. SPIE **7945**, 194 (2011).
12. H. Wu, X. Yin, L. Dong, *et al.*, Appl. Phys. Lett. **110**, 121104 (2017).
13. Q. Zhang, J. Chang, Z. Cong, *et al.*, IEEE Photonics J. **10**, 6804308 (2018).
14. A. Sampaolo, P. Patimisco, M. Giglio, *et al.*, Anal. Chim. Acta **1202**, 338894 (2022).
15. T. Steinle, F. Mörz, A. Steinmann, *et al.*, Opt. Lett. **41**, 4863 (2016).
16. L. Schmid, F. Kadriu, S. Kuppel, *et al.*, AIP Adv. **14**, 105328 (2024).
17. M. Lassen, L. Lamard, Y. Feng, *et al.*, Opt. Lett. **41**, 4118 (2016).
18. A. Ngai, S. T. Persijn, I. D. Lindsay, *et al.*, Appl. Phys. B **89**, 123 (2007).
19. J. B. Christensen, D. Balslev-Harder, L. Nielsen, *et al.*, Molecules **26**, 609 (2021).
20. J. B. Christensen, L. Høgstedt, S. M. M. Friis, *et al.*, Sensors **20**, 4725 (2020).
21. I. Gordon, L. Rothman, R. J. Hargreaves, *et al.*, J. Quant. Spectrosc. Radiat. Transfer **277**, 107949 (2022).
22. R. Kochanov, I. Gordon, L. Rothman, *et al.*, J. Quant. Spectrosc. Radiat. Transfer **177**, 15 (2016).
23. A. J. Jerri, Proc. IEEE **65**, 1565 (1977).